

Anomalous acoustic plasmons in two-dimensional over-tilted Dirac bands

Chang-Xu Yan,^{1,*} Furu Zhang,^{2,*} Chao-Yang Tan,^{1,*} Hao-Ran Chang,^{1,3,†} Jianhui Zhou,^{4,‡} Yugui Yao,⁵ and Hong Guo³

¹*Department of Physics, Institute of Solid State Physics and Center for Computational Sciences, Sichuan Normal University, Chengdu, Sichuan 610066, China*

²*Department of Mechanics and Engineering Science at College of Engineering, Peking University, Beijing 100871, P. R. China*

³*Department of Physics, McGill University, Montreal, Quebec H3A 2T8, Canada*

⁴*Anhui Key Laboratory of Condensed Matter Physics at Extreme Conditions, High Magnetic Field Laboratory, HFIPS, Anhui, Chinese Academy of Sciences, Hefei 230031, P. R. China*

⁵*Key Laboratory of Advanced Optoelectronic Quantum Architecture and Measurement (MOE), School of Physics, Beijing Institute of Technology, Beijing 100081, China*

The over-tilting of type-II Dirac cones has led to various fascinating quantum phenomena. Here we find two anomalous acoustic plasmons (AAPs) are dictated by the distinct geometry of two-dimensional (2D) type-II Dirac cones, far beyond the conventional \sqrt{q} plasmon. One AAP originates from the strong hybridization of two pockets at one Dirac point, whereas the other is attributed to the significant enhancement of the band correlation around the open Fermi surface. Remarkably, the plasmons exhibit valley-dependent chirality along the tilting direction due to the chiral electron dispersion. Meanwhile, we discuss the tunability of plasmon dispersion and lifetime by tuning the gap and dielectric substrate. Our work provides a promising way to generate the novel plasmons in Dirac materials.

Introduction.—Plasmon, the elementary excitation of electron liquids due to long-range Coulomb interaction, is a key ingredient of the emergent field of plasmonics [1, 2] and spintronics [3]. Recently, plasmons of Dirac fermions with linear dispersion have been extensively investigated in various contents, such as graphene-like systems [4–10], surface states of three-dimensional (3D) topological insulators [3, 11–19], 3D Dirac/Weyl semimetals [20–32], and topological nodal line semimetals [33–37]. Interestingly, the time-reversal symmetry breaking due to the external magnetic fields or spontaneous magnetization plays a crucial role in the creation of chiral or nonreciprocal plasmons [38–42], facilitating the chiral optical responses. However, the studies of generation and manipulation of novel plasmons with respect to the emergent Lorentz invariance in low-dimensional Dirac materials possessing high tunability of carrier density and/or background dielectric constant are rarely reported.

It has been shown that, in contrast to type-I Dirac cones [Fig. 1(a)] with the point-like Fermi surface [43–46], the over-tilting of type-II Dirac cones [Fig. 1(b)] would break the Lorentz invariance and leads to mixed Dirac pockets at the Dirac nodes [47]. Moreover, type-II Dirac/Weyl semimetals have been predicted to support a variety of novel electromagnetic responses [48–51] whose direct experimental evidences are still lacking. Surprisingly, recent works exhibited that the tilting parameter can be largely tuned by delicate strains, triggering transitions between type-I and type-II Dirac semimetals along with the dramatic changes of electronic states [47, 52]. Here we demonstrate that the alterable tilting of Dirac cones can be a new control knob of plasmons dictated by the unique geometry of type-II Fermi surface in a vari-

ety of two-dimensional (2D) Dirac materials, including the layered organic conductor α -(BEDT-TTF)₂I₃ [53–55], monolayer of transition metal dichalcogenides [56], and 8-*Pmmn* borophene [57–61] that possess multiple valleys in the Brillouin zone.

In this work, we find the tilting of Dirac cones could give rise to three distinct tunable plasmons rather than a conventional intraband plasmon in 2D type-II Dirac materials. We reveal their origins in terms of band correlations within a new momentum-space two-component Dirac model. These plasmons propagating in the tilting direction are valley-dependent and chiral due to the chiral electron dispersion. In addition, increasing the background dielectric constant could shift the two higher frequency plasmons to lower frequency and change their lifetime, while increasing energy gap through electrical gating could merge them into one.

Model.—We begin with the effective Hamiltonian for a pair of 2D massive Dirac cones with tilting in the y -direction [55, 56, 59, 62]

$$H_{\chi}(\mathbf{k}) = \chi v_t k_y \tau_0 + \chi v_F k_x \tau_1 + v_F k_y \tau_2 + \chi \Delta \tau_3, \quad (1)$$

where v_F is the Fermi velocity, v_t denotes the band tilting, $\chi = \pm$ labels two valleys K_{χ} , Δ stands for the magnitude of mass which may associate with the strength of intrinsic spin-orbit coupling or the gap due to symmetry breaking of spatial inversion, and the Planck's constant is set to be $\hbar = 1$. Additionally, the unit matrix τ_0 and Pauli matrix τ_i (with $i = 1, 2, 3$) act upon the pseudo-spin space. The eigenvalues of Eq. (1) are given as

$$E_{\lambda}^{\chi}(\mathbf{k}) = \chi v_t k_y + \lambda \sqrt{v_F^2 (k_x^2 + k_y^2) + \Delta^2}, \quad (2)$$

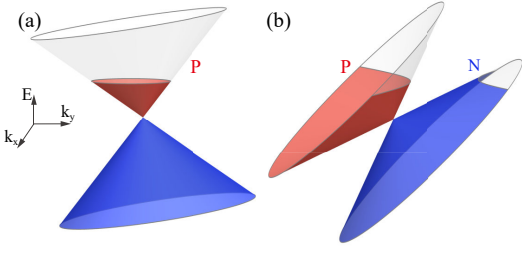


Figure 1. The energy dispersion and Fermi surface of the K_+ valley for (a) type-I Dirac semimetal and (b) type-II Dirac semimetal. The Fermi surface consists of (a) only one closed pocket (pocket-P) or (b) two open pockets (pocket-P and pocket-N). The Dirac node in the K_- valley tilts oppositely.

where $\lambda = \pm$ are band indices. Without loss of any generality, we at first focus on the gapless Dirac semimetals and discuss the influence of energy gap later.

Tuning the tilting parameter $t \equiv v_t/v_F$, the Dirac semimetal would undergo a phase transition from type-I ($0 \leq t < 1$) Dirac semimetal to type-II ($t > 1$) Dirac semimetal. Remarkably, each valley in the type-II Dirac semimetal possesses two open Fermi surfaces consisting of pocket-P ($\lambda = +$) and pocket-N ($\lambda = -$) characterized by distinct Fermi velocity along the tilting direction [Fig. 1(b)], in contrast to one closed elliptic Fermi surface, which consists of only one Dirac pocket in the type-I Dirac semimetal [Fig. 1(a)]. The highly anisotropic band structures and very distinct Fermi surfaces in the type-II Dirac semimetal would impose significant impacts on the plasmons.

Anomalous plasmons.—In order to reveal the nature of plasmon excitations for the type-II Fermi surface, we propose a model for tilted Dirac cones with multiple pockets in momentum space by generalizing the Das Sarma-Madhukar model originally describing the two-component plasmons made of spatially-separated conventional 2D electron gases [63]. Accordingly, the total dielectric tensor takes

$$\varepsilon_{\rho\lambda}(\mathbf{q}, \omega) = \delta_{\rho\lambda} - V_{\rho\lambda}(\mathbf{q}) \sum_{\chi=\pm} \Pi_{\lambda}^{\chi}(\mathbf{q}, \omega), \quad (3)$$

where ρ and λ are band indices. In this work, we focus on the electron correlations within each single Dirac point K_{χ} due to the large separation between K_+ and K_- in momentum space. For the multiple component plasmons in momentum space, the Coulomb interaction between carriers in different bands is taken to be $V_{\rho\lambda}(\mathbf{q}) = V_q$, where $V_q = 2\pi e^2/\kappa q$ is the Fourier transform of 2D Coulomb interaction with κ the effective dielectric constant and $q = |\mathbf{q}| = \sqrt{q_x^2 + q_y^2}$. The polarization function related to the band λ around Dirac node K_{χ} reads

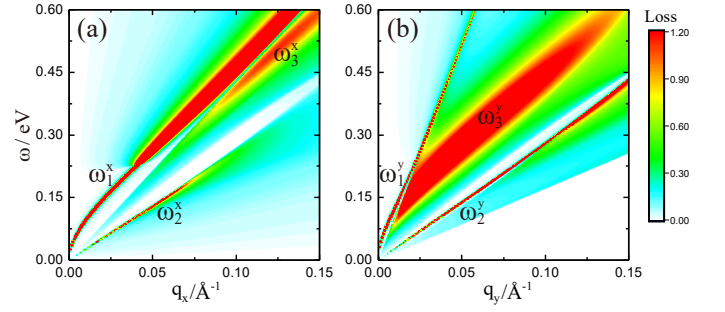


Figure 2. Plasmon dispersions from the EELF $\text{Loss}(\mathbf{q}, \omega)$. (a) the wave vector $\mathbf{q} = (q_x, 0)$ is perpendicular to the tilting direction and (b) the wave vector $\mathbf{q} = (0, q_y)$ is parallel to the tilting direction. Other parameters are taken to be $v_F = 0.65 \times 10^6$ m/s, $t = 1.4$, $\mu = 0.25$ eV and $\kappa = 15$ [67].

$$\begin{aligned} \Pi_{\lambda}^{\chi}(\mathbf{q}, \omega) &= \sum_{\lambda'=\pm\lambda} \int \frac{d^2\mathbf{k}}{(2\pi)^2} \mathcal{F}_{\lambda\lambda'}^{\chi}(\mathbf{k}, \mathbf{k}') \\ &\times \frac{n_F[E_{\lambda}^{\chi}(\mathbf{k})] - n_F[E_{\lambda'}^{\chi}(\mathbf{k}')] }{\omega + E_{\lambda}^{\chi}(\mathbf{k}) - E_{\lambda'}^{\chi}(\mathbf{k}') + i\eta}, \end{aligned} \quad (4)$$

where $\mathcal{F}_{\lambda\lambda'}^{\chi}(\mathbf{k}, \mathbf{k}') = |\langle \chi, \lambda, \mathbf{k} | \chi, \lambda', \mathbf{k}' \rangle|^2$ represents the overlap between wave functions with $|\chi, \lambda, \mathbf{k}\rangle$ being the periodic part of Bloch wave function [17] and $\mathbf{k}' = \mathbf{k} + \mathbf{q}$, $n_F(x) = [\exp[\beta(x - \mu)] + 1]^{-1}$ is the Fermi distribution function with $\beta = 1/(k_B T)$ and μ the chemical potential. It is emphasized that $\Pi_{\lambda}^{\chi}(\mathbf{q}, \omega)$ is contributed not only from the intraband process ($\lambda' = +\lambda$) but also from the interband process ($\lambda' = -\lambda$) and that the total dielectric tensor $\varepsilon_{\rho\lambda}(\mathbf{q}, \omega)$ receives contributions from both K_+ and K_- valleys. The condition for existence of collective modes is determined by the pole of the inverse of dielectric matrix $\varepsilon_{\rho\lambda}(\mathbf{q}, \omega)$, leading to an effective dielectric function

$$\varepsilon(\mathbf{q}, \omega) \equiv 1 - V_q \sum_{\chi=\pm} \sum_{\lambda=\pm} \Pi_{\lambda}^{\chi}(\mathbf{q}, \omega). \quad (5)$$

The plasmon excitations can be equivalently identified by peaks in the electron energy-loss function (EELF), defined as the negative imaginary part of the inverse dielectric function, $\text{Loss}(\mathbf{q}, \omega) = \text{Im}[-1/\varepsilon(\mathbf{q}, \omega)]$, which can be probed in various spectroscopy techniques, such as the electron energy-loss spectroscopy [64], scattering-type scanning near-field optical microscopy [65], and Fourier transform infrared spectroscopy [66].

When the wave vector is perpendicular to [Fig. 2(a)] or parallel to [Fig. 2(b)] the tilting direction, there are three distinct plasmons [68] rather than one single conventional plasmon in 2D metals, doped semiconductors, and semimetals [69]. First, the plasmon $\omega_1^{x/y}(q)$ is a conventional mode that obeys the \sqrt{q} law in the small wave

vector regime, which is a common feature of plasmons in 2D metallic systems [70]. Second, the first unusual plasmon $\omega_2^{x/y}(q)$ is an acoustic mode linear in q which ubiquitously appears in the type-II Dirac semimetal. More interestingly, the intermediate frequency plasmon $\omega_3^{x/y}(q)$ near the \sqrt{q} plasmon is quite unconventional, which has yet been discussed before in the conventional electron systems [69] and Dirac materials [28, 35]. Note that the plasmon with q -linear dispersion $\omega_3^{x/y}(q)$ usually hides as a shoulder in the region of intraband single particle excitation (SPE), hence dubbed the hidden plasmon in this work. Next we would examine the two anomalous acoustic plasmons (AAPs), $\omega_2(q)$ and $\omega_3(q)$.

Origin of plasmons.—To unveil the origins of these plasmons in the type-II Dirac semimetals, we perform analysis based on the band correlations within the momentum-space two-component Dirac fermion model. Firstly, we consider the three plasmons $\omega_{1,2,3}^y(q)$ in Fig. 2(b). Numerical results of the EELF clearly reveal the three plasmon peaks in the type-II Dirac semimetals are dominated by the band correlation within the K_+ valley, while the K_- valley does not contribute measurable signature [Figs. 3(a,b)]. Thus, the plasmon modes exhibit valley-dependent chirality, which can be well understood within the chiral energy dispersion. Since along the tilting direction, the carriers that bear the type-II Dirac semimetal are essentially the 1D chiral Dirac fermions similar to the edge state in the quantum anomalous Hall system [71, 72] and the corresponding energy dispersion is odd in k_y , that is, $E_\lambda^X(0, k_y) = v_F(\chi t k_y + \lambda |k_y|)$ [see the red and blue boundaries in Fig. 3(c) for $\chi = +$ and $t > 1$]. The resulting band correlations with $\mathbf{q} = (0, q_y)$ can be achieved for supporting plasmon excitations in a given Dirac cone or valley (for example K_+), but not in the other valley with opposite tilting K_- . On the contrary, when the wave vector $\mathbf{q} = (q_x, 0)$ is perpendicular to the tilting direction, the resulting three plasmons $\omega_{1,2,3}^x(q)$ in the type-II Dirac semimetals [Fig. 2(a)] are contributed equally by two valleys with opposite tilting, independent of valley-selection, see the Supplemental Materials (SM) [73]. Hence, we could focus on the contribution from the K_+ valley hereafter.

The plasmons $\omega_1^x(q)$ and $\omega_1^y(q)$ are dominated by the intraband correlations within pocket-P due to the difference between pocket-P and pocket-N in size and velocity, as shown in the SM [73] and Figs. 3(c,d). The gapped acoustic plasmons $\omega_2^x(q)$ and $\omega_2^y(q)$ linear in q , similar to the gapless Pines' demon [74], originate from the strong hybridization between intraband correlations from two pockets with different velocities [see the SM [73] and Figs. 3(c,d)]. Furthermore, it is worthy to emphasize that the AAP $\omega_2^x(q)$ in Fig. 2(a) is absent in the type-I Dirac semimetal since the plasmons therein become degenerate, sharing the same velocity [75]. Fitting the numerical result leads to the approximate dis-

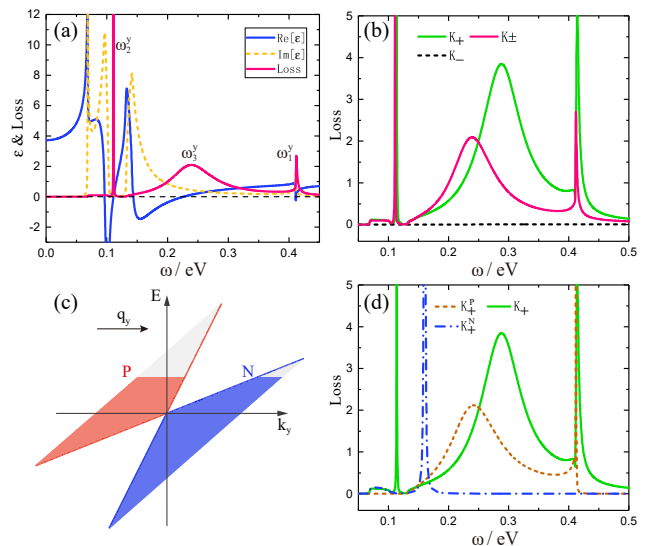


Figure 3. (a) Three plasmons are confirmed by the EELF and dielectric functions. (b) Three plasmons are contributed dominantly by the K_+ valley. (c) Schematic diagram of electron excitations in pocket-P ($\lambda = +$) and pocket-N ($\lambda = -$) at the K_+ valley. (d) Origin of plasmon peaks in terms of band correlations. The wave vector is $\mathbf{q} = (0, q_y)$ with $q_y = 0.04 \text{ \AA}^{-1}$.

persion of the acoustic plasmons $\omega_2^x(q) \approx \sqrt{1 - 1/t^2} v_F q$ and $\omega_2^y(q) \approx (t - 1/t) v_F q$, which clearly imply that the tilting can be used to tune the velocity of plasmon excitations [73]. In contrast to the gapless acoustic plasmon in the classical two-component model [63], the gap of the AAP here originates from the finite-range Coulomb interaction.

We turn to exploring the nature of $\omega_3^{x/y}(q)$, which are dominated by the intraband correlations of electrons in the pocket-P [see Figs. 3(c, d)], and lie in its intraband SPE [see Fig. 2]. To track which part of electrons around Fermi surfaces is responsible for activating this hidden plasmon, two subsets of $S_P = \{\mathbf{k} \in \mathbb{R}^2 | E_+^+(\mathbf{k}') > \mu > E_+^+(\mathbf{k})\}$ around K_+^P are defined as $T_1^P = \{\mathbf{k} \in S_P | \Delta E_P^+(\mathbf{k}, \mathbf{q}) < \omega_c(\mathbf{q})\}$ and $T_2^P = \{\mathbf{k} \in S_P | \omega_c(\mathbf{q}) < \Delta E_P^+(\mathbf{k}, \mathbf{q})\}$, where $\omega_c(\mathbf{q})$ denotes a specified frequency and $\Delta E_P^+(\mathbf{k}, \mathbf{q}) = E_+^+(\mathbf{k}') - E_+^+(\mathbf{k})$. We further recast the characteristic equation for plasmons as

$$\mathcal{I}_1^P + \mathcal{I}_2^P \approx 1/V_q, \quad (6)$$

where

$$\mathcal{I}_i^P \equiv \int_{\mathbf{k} \in T_i^P} \frac{d^2 \mathbf{k}}{(2\pi)^2} \frac{\mathcal{S}_P(\mathbf{k}, \mathbf{k}')}{\omega_c(\mathbf{q}) - \Delta E_P^+(\mathbf{k}, \mathbf{q})}, \quad (7)$$

with $\mathcal{S}_P(\mathbf{k}, \mathbf{k}') = \mathcal{F}_{++}^+(\mathbf{k}, \mathbf{k}') \Theta [E_+^+(\mathbf{k}') - \mu] \Theta [\mu - E_+^+(\mathbf{k})]$ and $i = 1, 2$.

For a given \mathbf{q} , a hyperbolic strip region defined by the condition $\mathcal{S}_P(\mathbf{k}, \mathbf{k}') > 0$ is divided by the contour corresponding to specified frequency $\Delta E_{++}^+(\mathbf{k}, \mathbf{q}) = \omega_c(\mathbf{q})$

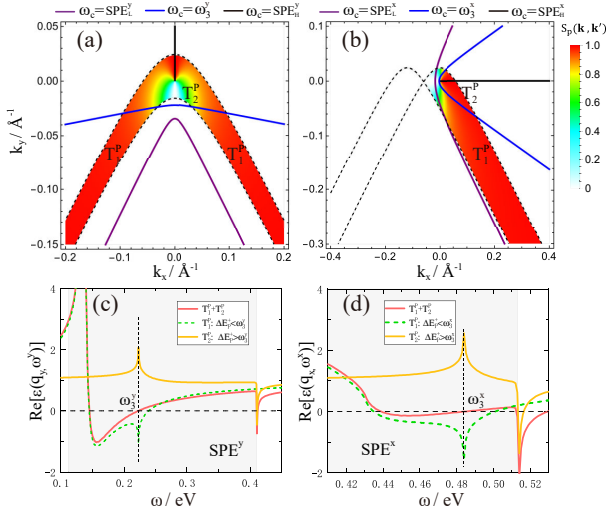


Figure 4. Origin of the intermediate frequency plasmons $\omega_3^{x/y}(q)$. $S_P(\mathbf{k}, \mathbf{k}')$ of the electrons in band $E_+^+(\mathbf{k})$ with a wave vector (a) $q_y = 0.04 \text{ \AA}^{-1}$ and (b) $q_x = 0.12 \text{ \AA}^{-1}$. The solid contours correspond to specified frequencies defined by $\Delta E_{\text{P}}^+(\mathbf{k}, \mathbf{q}) = \omega_c(\mathbf{q})$. The real part of dielectric functions $\text{Re}[\varepsilon(\mathbf{q}, \omega)]$ contributed by different processes are shown in (c) for $\mathbf{q} = (q_x, 0)$ and (d) for $\mathbf{q} = (0, q_y)$, respectively.

[see Figs. 4(a, b)], where T_1^{P} represents the part of strip region with open boundary due to the over-tilting while T_2^{P} denotes the part of strip region with closed boundary. Since $\frac{1}{v_q}$ is always positive, a plasmon can emerge when $\mathcal{I}_1^{\text{P}} + \mathcal{I}_2^{\text{P}} \geq 0$, in which the positive term is favorable to enhance the formation of plasmon while the negative term tends to suppress the formation of plasmon. When $\omega_c(\mathbf{q})$ is close to $\omega_3^{x/y}(q)$, the competition between the positive term \mathcal{I}_1^{P} from T_1^{P} and the negative term \mathcal{I}_2^{P} from T_2^{P} yields $\omega_3^{x/y}(q)$, indicating the strip region with open boundary T_1^{P} accounts for the appearance of $\omega_3^{x/y}(q)$, which is the characteristic feature of 2D type-II Dirac semimetal [Figs. 4(c,d)]. The nature of the thin-strip region supporting plasmon ω_3^y might be responsible to its linear dispersion, instead of the usual hybridization mechanism of different carriers. The case in the x-direction [see Fig. 4(b)] is similar, but the valid overlap region is about half of the case in the y-direction. Accordingly, $\omega_3^x(q)$ becomes weak compared with $\omega_3^y(q)$, which is in line with Figs. 2. Thus, the AAPs $\omega_3^{x/y}(q)$ activated by the over-tilting can be regarded as an unambiguous evidence of 2D type-II Dirac semimetals.

Manipulations of plasmons.—Let us turn to the impacts of energy gap and dielectric background on the plasmon modes in 2D type-II Dirac cones. With increasing the magnitude of energy gap (from $\Delta = 0$ to $\Delta = 0.24$ eV), the two higher frequency plasmons $\omega_1^y(q)$ and $\omega_3^y(q)$ would eventually merge into one strong plasmon [Fig. 5(a)]. In addition, increasing the effective

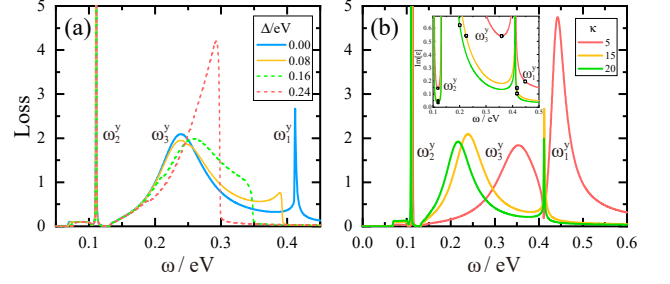


Figure 5. Impacts of (a) energy gap and (b) dielectric constant on plasmon modes $\omega_1^y(q)$, $\omega_2^y(q)$, and $\omega_3^y(q)$ for the wave vector $\mathbf{q} = (0, q_y)$ with $q_y = 0.04 \text{ \AA}^{-1}$. Other parameters are set to be $\kappa = 15$ in (a) and $\Delta = 0$ in (b). The imaginary part of $\varepsilon(\mathbf{q}, \omega)$ is shown in the inset of (b), where the circles denote the corresponding plasmon frequencies for different dielectric constants.

dielectric constant would continuously shift the peaks of the two higher frequency plasmons to lower frequency [Fig.5(b)], and change their lifetime [see the inset in Fig. 5(b)]. Interestingly, the peak of the lowest plasmon $\omega_2^y(q)$ remains almost unchanged against the change of energy gap or dielectric background [Fig. 5], but the lifetime of this plasmon is strengthened with increasing the dielectric constant [see the inset in Fig. 5(b)]. In fact, the magnitude of energy gap can be effectively modified by the gate voltages [56, 76], and the dielectric constant can be changed with different substrates, allowing us to manipulate the plasmon dispersions. The highly tunable plasmons would enable promising applications of 2D Dirac materials in plasmonics.

Conclusions.—In summary, we demonstrated that the tunable over-tilting of 2D Dirac cones leads to two AAPs associated with the distinct geometry of Fermi surface in type-II Dirac semimetals. One of the AAPs results from the strong hybridization of two pockets at a common Dirac point. Notably, this over-tilting enhances the band correlation to activate a strong unusual plasmon $\omega_3^{x/y}(q)$ that could characterize type-II Dirac bands. Moreover, the unique chiral electron-hole excitations along the tilting direction yield valley-nonreciprocity of plasmon modes. Thus, we hope that the present predictions would inspire immediate experimental investigations of the novel plasmons in various Dirac materials and their plasmonic applications.

The authors thank J. W. Liu for useful discussions. This work was supported by the National Key R&D Program of China (Grant No. 2020YFA0308800) and by the National Natural Science Foundation of China under Grants (No. 11547200 and No. 12174394), the China Postdoctoral Science Foundation (Grant No. 2019M650583). H.G. and H.-R.C. were also supported by the NSERC of Canada and the FQRNT of Quebec (H.G.). J.Z. was also supported by the High Magnetic Field Laboratory of Anhui Province. We thank the High

Performance Computing Centers at Sichuan Normal University, McGill University, and Compute Canada.

* These authors contributed equally to this work.

† hrchang@mail.ustc.edu.cn

‡ jhzhou@hmfl.ac.cn

- [1] D. Pines, *Elementary Excitations in Solids: Lectures on Protons, Electrons, and Plasmons*, Advanced book classics (Advanced Book Program, Perseus Books, 1999).
- [2] S. Maier, *Plasmonics: Fundamentals and Applications* (Springer US, 2010).
- [3] S. Raghu, S. B. Chung, X.-L. Qi, and S.-C. Zhang, *Phys. Rev. Lett.* **104**, 116401 (2010).
- [4] B. Wunsch, T. Stauber, F. Sols, and F. Guinea, *New Journal of Physics* **8**, 318 (2006).
- [5] E. H. Hwang and S. Das Sarma, *Phys. Rev. B* **75**, 205418 (2007).
- [6] M. Polini, R. Asgari, G. Borghi, Y. Barlas, T. Peregr-Barnea, and A. H. MacDonald, *Phys. Rev. B* **77**, 081411 (2008).
- [7] S. Gangadharaiyah, A. M. Farid, and E. G. Mishchenko, *Phys. Rev. Lett.* **100**, 166802 (2008).
- [8] G. Cheng, W. Qin, M.-H. Lin, L. Wei, X. Fan, H. Zhang, S. Gwo, C. Zeng, J. G. Hou, and Z. Zhang, *Phys. Rev. Lett.* **119**, 156803 (2017).
- [9] J. Wang, X. Sui, S. Gao, W. Duan, F. Liu, and B. Huang, *Phys. Rev. Lett.* **123**, 206402 (2019).
- [10] J. Cao, H. A. Fertig, and L. Brey, *Phys. Rev. Lett.* **127**, 196403 (2021).
- [11] P. Di Pietro, M. Ortolani, O. Limaj, A. Di Gaspare, V. Giliberti, F. Giorgianni, M. Brahlek, N. Bansal, N. Koirala, S. Oh, P. Calvani, and S. Lupi, *Nature Nanotech* **8**, 556 (2013).
- [12] S. Juergens, P. Michetti, and B. Trauzettel, *Phys. Rev. Lett.* **112**, 076804 (2014).
- [13] J.-Y. Ou, J.-K. So, G. Adamo, A. Sulaev, L. Wang, and N. I. Zheludev, *Nat. Commun.* **5** (2014).
- [14] A. Kogar, S. Vig, A. Thaler, M. H. Wong, Y. Xiao, D. Reig-i Plessis, G. Y. Cho, T. Valla, Z. Pan, J. Schneeloch, R. Zhong, G. D. Gu, T. L. Hughes, G. J. MacDougall, T.-C. Chiang, and P. Abbamonte, *Phys. Rev. Lett.* **115**, 257402 (2015).
- [15] A. Politano, V. M. Silkin, I. A. Nechaev, M. S. Vitiello, L. Viti, Z. S. Aliev, M. B. Babanly, G. Chiarello, P. M. Echenique, and E. V. Chulkov, *Phys. Rev. Lett.* **115**, 216802 (2015).
- [16] X. Jia, S. Zhang, R. Sankar, F.-C. Chou, W. Wang, K. Kempa, E. W. Plummer, J. Zhang, X. Zhu, and J. Guo, *Phys. Rev. Lett.* **119**, 136805 (2017).
- [17] F. Zhang, J. Zhou, D. Xiao, and Y. Yao, *Phys. Rev. Lett.* **119**, 266804 (2017).
- [18] A. Shvonski, J. Kong, and K. Kempa, *Phys. Rev. B* **99**, 125148 (2019).
- [19] T. Wei, Y. Liu, P. Cui, X. Li, and Z. Zhang, *Phys. Rev. B* **105**, 205408 (2022).
- [20] S. Das Sarma and E. H. Hwang, *Phys. Rev. Lett.* **102**, 206412 (2009).
- [21] I. Panfilov, A. A. Burkov, and D. A. Pesin, *Phys. Rev. B* **89**, 245103 (2014).
- [22] J. Zhou, H.-R. Chang, and D. Xiao, *Phys. Rev. B* **91**, 035114 (2015).
- [23] J. Hofmann and S. Das Sarma, *Phys. Rev. B* **91**, 241108 (2015).
- [24] D. E. Kharzeev, R. D. Pisarski, and H.-U. Yee, *Phys. Rev. Lett.* **115**, 236402 (2015).
- [25] E. V. Gorbar, V. A. Miransky, I. A. Shovkovy, and P. O. Sukhachov, *Phys. Rev. Lett.* **118**, 127601 (2017).
- [26] A. Politano, G. Chiarello, B. Ghosh, K. Sadhukhan, C.-N. Kuo, C. S. Lue, V. Pellegrini, and A. Agarwal, *Phys. Rev. Lett.* **121**, 086804 (2018).
- [27] Z. Long, Y. Wang, M. Erukhimova, M. Tokman, and A. Belyanin, *Phys. Rev. Lett.* **120**, 037403 (2018).
- [28] K. Sadhukhan, A. Politano, and A. Agarwal, *Phys. Rev. Lett.* **124**, 046803 (2020).
- [29] X. Jia, M. Wang, D. Yan, S. Xue, S. Zhang, J. Zhou, Y. Shi, X. Zhu, Y. Yao, and J. Guo, *New J. Phys.* **22**, 103032 (2020).
- [30] C. Wang, Y. Sun, S. Huang, Q. Xing, G. Zhang, C. Song, F. Wang, Y. Xie, Y. Lei, Z. Sun, and H. Yan, *Phys. Rev. Appl.* **15**, 014010 (2021).
- [31] S. Heidari, D. Culcer, and R. Asgari, *Phys. Rev. B* **103**, 035306 (2021).
- [32] A. N. Afanasiev, A. A. Greshnov, and D. Svintsov, *Phys. Rev. B* **103**, 205201 (2021).
- [33] Z. Yan, P.-W. Huang, and Z. Wang, *Phys. Rev. B* **93**, 085138 (2016).
- [34] J.-W. Rhim and Y. B. Kim, *New J. Phys.* **18**, 043010 (2016).
- [35] S. Xue, M. Wang, Y. Li, S. Zhang, X. Jia, J. Zhou, Y. Shi, X. Zhu, Y. Yao, and J. Guo, *Phys. Rev. Lett.* **127**, 186802 (2021).
- [36] S. F. Islam and A. A. Zyuzin, *Phys. Rev. B* **104**, 245301 (2021).
- [37] Y. Shao, A. J. Sternbach, B. S. Y. Kim, A. A. Rikhter, X. Xu, U. De Giovannini, R. Jing, S. H. Chae, Z. Sun, S. H. Lee, Y. Zhu, Z. Mao, J. Hone, R. Queiroz, A. J. Millis, P. J. Schuck, A. Rubio, M. M. Fogler, and D. N. Basov, arXiv:2206.01828 (2022).
- [38] A. Kumar, A. Nemilentsau, K. H. Fung, G. Hanson, N. X. Fang, and T. Low, *Phys. Rev. B* **93**, 041413 (2016).
- [39] J. C. W. Song and M. S. Rudner, *Proc. Natl. Acad. Sci. U.S.A.* **113**, 4658 (2016).
- [40] A. C. Mahoney, J. I. Colless, L. Peeters, S. J. Pauka, E. J. Fox, X. Kou, L. Pan, K. L. Wang, D. Goldhaber-Gordon, and D. J. Reilly, *Nature Communications* **8**, 1836 (2017).
- [41] X. Lin, Z. Liu, T. Stauber, G. Gómez-Santos, F. Gao, H. Chen, B. Zhang, and T. Low, *Phys. Rev. Lett.* **125**, 077401 (2020).
- [42] H. Schlömer, Z. Jiang, and S. Haas, *Phys. Rev. B* **103**, 115116 (2021).
- [43] X. Wan, A. M. Turner, A. Vishwanath, and S. Y. Savrasov, *Phys. Rev. B* **83**, 205101 (2011).
- [44] H. Weng, R. Yu, X. Hu, X. Dai, and Z. Fang, *Advances in Physics* **64**, 227 (2015).
- [45] N. P. Armitage, E. J. Mele, and A. Vishwanath, *Rev. Mod. Phys.* **90**, 015001 (2018).
- [46] B. Q. Lv, T. Qian, and H. Ding, *Rev. Mod. Phys.* **93**, 025002 (2021).
- [47] A. A. Soluyanov, D. Gresch, Z. Wang, Q. Wu, M. Troyer, X. Dai, and B. A. Bernevig, *Nature* **527**, 495 (2015).
- [48] M. Udagawa and E. J. Bergholtz, *Phys. Rev. Lett.* **117**, 086401 (2016).
- [49] T. E. O'Brien, M. Diez, and C. W. J. Beenakker, *Phys. Rev. Lett.* **116**, 236401 (2016).

- [50] S. Tchoumakov, M. Civelli, and M. O. Goerbig, *Phys. Rev. Lett.* **117**, 086402 (2016).
- [51] Z.-M. Yu, Y. Yao, and S. A. Yang, *Phys. Rev. Lett.* **117**, 077202 (2016).
- [52] X.-P. Li, K. Deng, B. Fu, Y. Li, D.-S. Ma, J. Han, J. Zhou, S. Zhou, and Y. Yao, *Phys. Rev. B* **103**, L081402 (2021).
- [53] K. Bender, I. Hennig, D. Schweitzer, K. Dietz, H. Endres, and H. J. Keller, *Molecular Crystals and Liquid Crystals* **108**, 359 (1984).
- [54] S. Katayama, A. Kobayashi, and Y. Suzumura, *Journal of the Physical Society of Japan* **75**, 054705 (2006).
- [55] M. Hirata, K. Ishikawa, K. Miyagawa, M. Tamura, C. Berthier, D. Basko, A. Kobayashi, G. Matsuno, and K. Kanoda, *Nat. Commun.* **7**, 12666 (2016).
- [56] X. Qian, J. Liu, L. Fu, and J. Li, *Science* **346**, 1344 (2014).
- [57] X.-F. Zhou, X. Dong, A. R. Oganov, Q. Zhu, Y. Tian, and H.-T. Wang, *Phys. Rev. Lett.* **112**, 085502 (2014).
- [58] A. J. Mannix, X.-F. Zhou, B. Kiraly, J. D. Wood, D. Alducin, B. D. Myers, X. Liu, B. L. Fisher, U. Santiago, J. R. Guest, M. J. Yacaman, A. Ponce, A. R. Oganov, M. C. Hersam, and N. P. Guisinger, *Science* **350**, 1513 (2015).
- [59] B. Feng, O. Sugino, R.-Y. Liu, J. Zhang, R. Yukawa, M. Kawamura, T. Iimori, H. Kim, Y. Hasegawa, H. Li, L. Chen, K. Wu, H. Kumigashira, F. Komori, T.-C. Chiang, S. Meng, and I. Matsuda, *Phys. Rev. Lett.* **118**, 096401 (2017).
- [60] Z. Jalali-Mola and S. A. Jafari, *Phys. Rev. B* **102**, 245148 (2020).
- [61] C. Lian, S.-Q. Hu, J. Zhang, C. Cheng, Z. Yuan, S. Gao, and S. Meng, *Phys. Rev. Lett.* **125**, 116802 (2020).
- [62] C.-Y. Tan, C.-X. Yan, Y.-H. Zhao, H. Guo, and H.-R. Chang, *Phys. Rev. B* **103**, 125425 (2021).
- [63] S. Das Sarma and A. Madhukar, *Phys. Rev. B* **23**, 805 (1981).
- [64] H. Ibach and D. L. Mills, *Electron energy loss spectroscopy and surface vibrations* (Academic Press New York, 1982).
- [65] N. C. H. Hesp, I. Torre, D. Rodan-Legrain, P. Novelli, Y. Cao, S. Carr, S. Fang, P. Stepanov, D. Barcons-Ruiz, H. Herzig Sheinfux, K. Watanabe, T. Taniguchi, D. K. Efetov, E. Kaxiras, P. Jarillo-Herrero, M. Polini, and F. H. L. Koppens, *Nat. Phys.* **17**, 1162 (2021).
- [66] A. Grigorenko, M. Polini, and K. Novoselov, *Nat. Photon.* **6**, 749 (2012).
- [67] For a finite Fermi level apart from the Dirac point, the qualitative features of three plasmons due to over-tilting of Dirac cones are not sensitive to the magnitude of the Fermi level. When the Fermi level crosses the Dirac point, the lowest frequency plasmon almost disappears due to over damping [73].
- [68] The calculation based on the equivalent tight-binding model also yields three plasmon modes and is in line with the results in Fig. (2) from the effective $k \cdot p$ model [73].
- [69] G. Giuliani and G. Vignale, *Quantum theory of the electron liquid* (Cambridge University Press, Cambridge, UK, 2005).
- [70] T. Ando, A. B. Fowler, and F. Stern, *Rev. Mod. Phys.* **54**, 437 (1982).
- [71] R. Yu, W. Zhang, H.-J. Zhang, S.-C. Zhang, X. Dai, and Z. Fang, *Science* **329**, 61 (2010).
- [72] C.-Z. Chang, J. Zhang, X. Feng, J. Shen, Z. Zhang, M. Guo, K. Li, Y. Ou, P. Wei, L.-L. Wang, *et al.*, *Science* **340**, 167 (2013).
- [73] See Supplemental Material for details about the fitting of the approximate dispersions of the lowest frequency acoustic plasmons, the comparison between the plasmons from the $k \cdot p$ model and those from the corresponding tight-binding model and the plasmon dispersions for negative chemical potential.
- [74] D. Pines, *Canadian Journal of Physics* **34**, 1379 (1956).
- [75] T. Nishine, A. Kobayashi, and Y. Suzumura, *Journal of the Physical Society of Japan* **80**, 114713 (2011).
- [76] S. Wu, V. Fatemi, Q. D. Gibson, K. Watanabe, T. Taniguchi, R. J. Cava, and P. Jarillo-Herrero, *Science* **359**, 76 (2018).